Finite-temperature Yang-Mills theories with the density of states method: Toward the continuum limit

Ed Bennett,[1,2,*] Biagio Lucini,[1,3,4,†] David Mason,[5,‡] Maurizio Piai,[2,6,§] Enrico Rinaldi,[7,‖] Davide Vadacchino,[8,¶] and Fabian Zierler[2,6,**]

(TELOS collaboration)

[1]*Swansea Academy of Advanced Computing, Swansea University (Bay Campus), Fabian Way, Swansea SA1 8EN, United Kingdom*
[2]*Centre for Quantum Fields and Gravity, Faculty of Science and Engineering, Swansea University, Singleton Park, SA2 8PP, Swansea, United Kingdom*
[3]*Department of Mathematics, Faculty of Science and Engineering, Swansea University (Bay Campus), Fabian Way, SA1 8EN Swansea, United Kingdom*
[4]*School of Mathematical Sciences, Queen Mary University of London, Mile End Road, London, E1 4NS, United Kingdom*
[5]*Jülich Supercomputing Centre, Forschungszentrum Jülich, D-52425 Jülich, Germany*
[6]*Department of Physics, Faculty of Science and Engineering, Swansea University, Singleton Park, SA2 8PP, Swansea, United Kingdom*
[7]*RIKEN Center for Interdisciplinary Theoretical and Mathematical Sciences (iTHEMS), RIKEN, 2-1 Hirosawa, Wako, Saitama, 351-0198, Japan*
[8]*Centre for Mathematical Sciences, University of Plymouth, Plymouth, PL4 8AA, United Kingdom*

(Received 3 October 2025; accepted 31 March 2026; published 24 April 2026)

A first-order, confinement/deconfinement phase transition appears in the finite temperature behavior of many non-Abelian gauge theories. These theories play an important role in proposals for completion of the Standard Model of particle physics, hence the phase transition might have occurred in the early stages of evolution of our Universe, leaving behind a detectable relic stochastic background of gravitational waves. Lattice field theory studies implementing the density of states method have the potential to provide detailed information about the phase transition, and measure the parameters determining the gravitational-wave power spectrum, by overcoming some of the challenges faced by importance-sampling methods. We assess this potential for a representative choice of Yang-Mills theory with $Sp(4)$ gauge group. We characterize its finite-temperature, first-order phase transition, in the thermodynamic (infinite volume) limit, for two different choices of number of sites in the compact time direction, hence taking the first steps toward the continuum limit extrapolation. We demonstrate the persistence of nonperturbative phenomena associated to the first-order phase transition: coexistence of states, metastability, latent heat, surface tension. We find consistency between several different strategies for the extraction of the volume-dependent critical coupling, hence assessing the size of systematic effects. We also determine the minimum choice of ratio between spatial and time extent of the lattice that allows one to identify the contribution of the surface tension to the free energy. We observe that this ratio scales nontrivially with the time extent of the lattice, and comment on the implications for future high-precision numerical studies.

DOI: 10.1103/ww6s-xw9z

[*]Contact author: e.j.bennett@swansea.ac.uk
[†]Contact author: b.lucini@qmul.ac.uk
[‡]Contact author: d.mason@fz-juelich.de
[§]Contact author: m.piai@swansea.ac.uk
[‖]Contact author: erinaldi.work@gmail.com
[¶]Contact author: davide.vadacchino@plymouth.ac.uk
[**]Contact author: fabian.zierler@swansea.ac.uk

I. INTRODUCTION

Finite-temperature, first-order phase transitions in gauge theories are critical to our understanding of particle physics and cosmology. Yet, their characterization on the lattice requires overcoming algorithmic and technological challenges. It is hence the subject of a vast literature, both for $SU(3)$ gauge theories—see for example the discussion in Ref. [1], the review [2], and references therein, in particular Refs. [3,4], but also Refs. [5–17] and Refs. [18–24]—and for other gauge groups, relevant for new physics [25–39].

Appealing extensions of the Standard Model (SM) of particle physics postulate the existence of new dark sectors [40–46], taking a variety of forms: composite dark matter models [47–56], strongly interacting massive particle models [57–69], dark dilaton effective field theories [70–72]. They address puzzles in the Standard Model of cosmology, such as observational evidence that dark energy and dark matter, that have no SM explanation, dominate our present Universe (see, e.g., the review in Ref. [73]). Even explaining the observed baryonic component requires a matter-antimatter asymmetry that admits no dynamical SM origin—see Refs. [74,75] for reviews, and references therein. In particular Refs. [76–83] show the failure of the Sakharov's out-of-equilibrium condition [84] for electroweak baryogenesis.

If the dark sector gauge theory undergoes, in the early Universe, a strong first-order phase transition, it leads to the emission of gravitational waves [85–90], potentially detectable by future experimental programs [91–108]—see also Ref. [109]. Appraising the viability of experimental searches necessitates a precise characterization of the physics in proximity of the transition, including a measurement of the parameters that control the gravitational wave (GW) power spectrum. Of particular interest are α, which is a measure of the strength of the transition, and β/H_* [107], where β corresponds to the duration of the phase transition and H_* is the Hubble parameter at the transition. The latent heat can be related to α and the bubble nucleation rate (and bubble surface tension) can be related to β/H_*.[1]

The main challenge for the direct lattice numerical calculation of these quantities (that act as input values in numerical packages such as PTPlot [107]) is that first-order phase transitions are accompanied by phase coexistence and metastability. These phenomena compromise ergodicity and detailed balance requirements of traditional importance-sampling techniques, based on Markov chain Monte Carlo update algorithms, and lead to critical slowing down [111]. Indirect routes can be pursued to estimate the power spectrum in strongly coupled theories [112–117], using effective Polyakov-loop theory [118–126] and matrix models [127–135]. Most recently, gauge-gravity duality techniques [136–139], adapted to capture confinement and chiral symmetry breaking [140–150], have also been used for the treatment of first-order phase transitions in strongly coupled field theories—see, e.g., Refs. [151–163].

This paper adopts a new, alternative strategy to gain direct access to the proximity of first-order phase transitions, that takes inspiration from flat histogram [111] and density of states [164] methods. The logarithmic linear relaxation (LLR) algorithm [165–168]—see also Ref. [169]—is precisely described in the body of the paper. The underlying idea is to scan the space of configurations with a density function inspired by the microcanonical (rather than canonical) ensemble in statistical mechanics, and treat on equal footing stable, metastable, as well as unstable configurations of the lattice system, overcoming the difficulties connected with importance sampling methods. A number of increasingly sophisticated analyses have already been performed, pertaining to Abelian gauge theories [167], and to $SU(3)$ theories at zero [168] and finite temperature [170–172]. Finite-temperature studies exist also for $Sp(4)$ [173], $SU(4)$ [174,175] and $SU(N_c)$ [176,177], all of which yield encouraging preliminary results.

We consider a non-Abelian gauge theory—the $Sp(4)$ Yang-Mills theory in four dimensions—characterize its finite-temperature deconfinement transition using the LLR algorithm, and perform the first scaling test to approach the continuum and infinite-volume limits. To this purpose, we discretize the theory on hypercubic lattices with varying number of sites on the temporal, $N_t = 4$ and $N_t = 5$, and spatial, N_s, directions, measure a set of observables, extrapolate them to the physical limits, and assess the magnitude of methodological systematic uncertainties. The free energy density of the theory displays its multivalued nature in a region of parameter space in proximity of the first-order phase transition. We estimate the critical couplings at finite volume, β_{CV}, (in the following referred to as critical couplings, for brevity) extracted in several complementary ways, with finite spatial volume of the lattice. We also measure the specific heat and surface tension. We study in detail how all the lattice observables converge to continuum field theory quantities in the limits of $N_s \to +\infty$ (the infinite-volume, or thermodynamic, limit) and $N_t \to +\infty$.

The TELOS collaboration has been carrying out a systematic program of lattice studies of the $Sp(2N)$ gauge theories, both in the pure gauge case [178–182], as well as in the presence of fermion matter fields [178,183–193], reshaping our understanding of these theories—see also the review in Ref. [194], as well as Refs. [68,195–197]. The $Sp(4)$ Yang-Mills theory is the most accessible and best understood one in this class, and hence a natural target of the present study, though our results are expected to be relevant also for the study of other gauge groups [see Ref. [172] for $SU(3)$]. The study presented in this paper uses some of the technology TELOS developed and made publicly available, such as the implementation within the HiRep code [198,199] of the adaptations needed for the

[1]Calculating the nucleation rate is itself a challenging task [110].

study of $Sp(N_c = 2N)$ theories [178,200], and the implementation of the heat bath and domain decomposition initially implemented for $SU(N_c)$ gauge groups [172,201], extended to symplectic gauge groups [173,202].

The paper is organized as follows. In Sec. II, we outline the methodology based on the density of states. We describe pedagogically the relevant aspects of the density of states methods, and the implementation of the LLR algorithm in the (continuum) field theory context of relevance. In Sec. III, we discuss the numerical lattice field theory of interest and the formulation of the LLR algorithm on a finite lattice. We report our new results in Sec. IV. This section contains also critical discussions, which include direct comparisons to the existing, published data, obtained with smaller time and space extents of the lattice. We conclude in Sec. V, by summarizing the main results of the study, and outlining future avenues for investigation. We collect some technical aspects of the numerical study in the Appendix.

II. FIELD THEORY FORMULATION OF THE LLR ALGORITHM

In this section, we introduce the density of states methodology for non-Abelian gauge theories, and its implementation in the LLR algorithm. The presentation is self-contained and pedagogical, and we refer to the literature for additional details [165–169]. We also discuss our implementation of the replica exchange, to enforce ergodicity, and comment on our estimation of errors.

A. Density of states

We write the partition function of the Yang-Mills gauge theory with group $Sp(2N)$, treated in isolation from any other fields (including SM ones) as follows:

$$Z(\beta) \equiv \int [DA] e^{-\beta S[A]}, \tag{1}$$

where $\beta \equiv 4N/g_0^2$, with g_0 the bare gauge coupling, and $[DA]$ the (Haar) measure. The Euclidean action, $S[A]$, is expressed as a function of the gauge fields, $A = \sum_B A_\mu^B T^B$, where T^B are the generators of the group, while

$$S[A] \equiv \int \mathrm{d}^4 x \mathrm{Tr}\left[\frac{1}{2} F_{\mu\nu}(x) F_{\mu\nu}(x)\right], \tag{2}$$

and the field-strength tensor is

$$F_{\mu\nu}(x) \equiv \partial_\mu A_\nu(x) - \partial_\nu A_\mu(x) + i[A_\mu(x), A_\nu(x)]. \tag{3}$$

Notice how we made explicit the dependence on β in the exponential weight, rather than in the action.

The expectation value of a generic operator, $O[A]$, that depends on the gauge fields, is

$$\langle O \rangle_\beta \equiv \frac{1}{Z(\beta)} \int [DA] O[A] e^{-\beta S[A]}. \tag{4}$$

This expression implicitly defines a probability density in the space of the fields, $\mathrm{d}P_\beta[A]$, taking the form

$$\mathrm{d}P_\beta(A) = \frac{1}{Z(\beta)} [DA] e^{-\beta S[A]}. \tag{5}$$

In the presence of a first-order transition, this probability density may show multiple, inequivalent stationary points, corresponding to coexisting phases. On the lattice, importance-sampling (Markov chain) algorithms have exponentially suppressed transition rates in Monte Carlo time between regions near different local maxima of the probability distribution. The resulting freezing of the updates near one of the local maxima introduces the aforementioned violations of ergodicity and detailed balance (hysteresis). Ultimately, the resulting critical slowing down [111] makes it unfeasible to overcome the problem with realistic amounts of computational resources.

The approach based upon the density of states, $\rho(E)$, is designed to overcome these challenges. One constrains the action, $S[A]$, to match the energy, $S[A] = E$,

$$\rho(E) \equiv \int [DA] \delta(S[A] - E), \tag{6}$$

and then rewrites the ensemble average of any operator that is only a function of the action $O(E = S[A])$ as[2]

$$\langle O \rangle_\beta = \frac{1}{Z(\beta)} \int \mathrm{d}E \rho(E) O(E) e^{-\beta E}. \tag{7}$$

The calculation of $\langle O \rangle_\beta$ for a value of β therefore requires determining the density of states, $\rho(E)$, at all values of the energy $S[A] = E$. As in the process we explore all values of E individually, there is no concern about transitions between inequivalent configurations (phases), that have different energy, E. The probability distribution density for a given energy is then written as

$$P_\beta(E) = \frac{1}{Z(\beta)} \rho(E) e^{-\beta E}. \tag{8}$$

This method can yield a precise determination of the critical coupling, since β is no longer a parameter entering the Monte Carlo calculations, but rather can be tuned freely once $\rho(E)$ has been determined numerically. The nontrivial algorithm leading to such determination is the subject of the next subsection.

[2]This approach can be generalized to other observables, such as the Polyakov loop, in which case additional information may be required—see, e.g., the discussion in Ref. [167].

B. Linear logarithmic relaxation (LLR)

When computing ensemble averages with Eq. (7), one finds that they are dominated by integrations over finite energy intervals. We use this empirical observation to guide our heuristic choice of the range $[E_{\min}, E_{\max}]$, which includes all such intervals, but requires deploying only limited amounts of computational resources, as we neglect exponentially suppressed contributions from other energies. A caveat to this approach is that it compromises the implementation of the third law of thermodynamics, which would require the continuous mapping of $\rho(E)$ to reach the low energy regime close to zero temperature. The drawback is the appearance of an arbitrary constant, to which we return shortly.

We cover the energy range, $[E_{\min}, E_{\max}]$, with intervals of finite width, $\Delta_E/2$,[3] centered around regularly spaced energies, $E_0^{(n)}$, for $n = 1, \ldots, N$. We characterize the density of states in terms of its logarithmic derivative, $a(E)$, defined as

$$a(E) \equiv \frac{\mathrm{d}}{\mathrm{d}E} \log \rho(E), \tag{9}$$

which we determine by modeling it with the approximation $\log \tilde{\rho}(E) \simeq \log \rho(E)$, consisting of a piecewise-linear function defined so that

$$\log \rho(E) \simeq \log \tilde{\rho}(E) \equiv a^{(n)}(E_0^{(n)} - E) + c^{(n)}, \quad \text{for } E \in \left[E_0^{(n)} - \frac{\Delta_E}{4}, E_0^{(n)} + \frac{\Delta_E}{4}\right]. \tag{10}$$

The determination of $\tilde{\rho}$ is then equivalent to the reconstruction of all $a^{(n)}$, and $c^{(0)}$. The coefficients $c^{(n)}$, with $n > 0$, are determined by requiring continuity. The first coefficient, $c^{(0)}$, is left undetermined by this approach, but as anticipated only results in an overall normalization of the partition function, $Z(\beta)$, that drops out of ensemble averages such as those in Eq. (7).

In order to illustrate how we determine the numerical values of $a^{(n)}$, we introduce the restricted expectation value, for which we use the double-bracket notation,

$$\langle\!\langle f \rangle\!\rangle_n(\hat{a}) \equiv \frac{1}{\mathcal{N}_n(\hat{a})} \int D[A] f[A] e^{-\hat{a}(S[A] - E_0^{(n)})} W(S[A] - E_0^{(n)}, \delta), \tag{11}$$

$$\text{where } \mathcal{N}_n(\hat{a}) \equiv \int D[A] e^{-\hat{a}(S[A] - E_0^{(n)})} W(S[A] - E_0^{(n)}, \delta), \tag{12}$$

$$\text{and} \quad W(x, \delta) \equiv \begin{cases} 1, & \text{if } -\delta/2 < x < \delta/2 \\ 0, & \text{otherwise} \end{cases}, \tag{13}$$

[3]We follow the notation from Ref. [173].

TABLE I. Characterization of the lattice studies used for this work. We report the lattice size, $N_t \times N_s^3$, the energy range, given in terms of the average plaquette, $[u_p^{\min}, u_p^{\max}]$, as well as the number of replicas/intervals, $N_{\text{rep}} = N$, and the number of repeats, N_{repeats}. We further report the total number of Newton-Raphson and Robbins-Monro iteration steps, N_{NR} and N_{RM}, respectively. We also include the ensembles from Ref. [173], for $N_t = 4$, which we use to recalculate all quantities considered in this paper to facilitate comparison with the new data at $N_t = 5$.

N_t	N_s	$u_p^{\min}$	$u_p^{\max}$	N_{rep}	N_{repeats}	n_{NR}	n_{RM}
5	48	0.588	0.592	48	25	10	60
5	48	0.588	0.592	96	25	10	50
5	56	0.588	0.592	128	25	10	50
5	56	0.588	0.592	48	25	10	50
5	56	0.588	0.592	96	25	10	50
5	64	0.588	0.592	95	20	7	50
5	72	0.588	0.592	95	20	11	50
5	80	0.588	0.59	64	20	15	30
4	20	0.565	0.58	64	20	10	300
4	24	0.565	0.58	64	20	10	300
4	28	0.565	0.58	64	20	10	200
4	40	0.568	0.576	128	25	10	100
4	48	0.568	0.576	128	26	10	100

for any function, $f(A)$, of the fields, A.[4] Here, $\hat{a}$ is a generic parameter, while $W(x, \delta)$ restricts the energy to an interval centered around x with fixed width, δ.

As the double-bracket expectation value, $\langle\!\langle f \rangle\!\rangle_n(\hat{a})$, in Eq. (11) can be explicitly rewritten in the form of Eq. (4), it can be calculated using standard Monte-Carlo techniques. But because the energy is restricted to an interval, this calculation (for sufficiently small choices of interval, δ) is not affected by the aforementioned challenges, due to possible metastability and phase coexistence. Furthermore, it can be shown that [165]

$$\langle\!\langle S[A] - E_0^{(n)} \rangle\!\rangle_n(\hat{a} = a^{(n)}) = 0. \tag{14}$$

This observation allows one to translate the problem of determining $a^{(n)}$ (and the density of states) into the algebraic solution of Eq. (14), for each interval labeled by n. We do so iteratively, with a combination of the Newton-Raphson (NR) and Robbins-Monro (RM) updates as defined below [203]—see also Table I for the exact number of the respective number of iterations. After estimating the derivative of $\langle\!\langle S[A] - E_0^{(n)} \rangle\!\rangle_n$ [165,167], we arrive at the iterative equation

[4]The double bracket in the notation reflects the fact that this object closely resembles the simultaneous application of microcanonical and canonical ensembles, as it amounts to restricting the integration to a narrow interval around a given value of the energy, $E_0^{(n)}$, but also to multiplying the integrand by a weight function depending exponentially on $S[A]$—an overall factor of $e^{\hat{a}E_0^{(n)}}$ drops from the ratio with the normalization, $\mathcal{N}_n(\hat{a})$.

$$a_{k+1}^{(n)} = a_k^{(n)} - \alpha_{k+1} \frac{12}{\delta^2} \langle\langle S[A] - E_0^{(n)} \rangle\rangle_n (a_k^{(n)}), \quad (15)$$

where $\alpha_k = 1$ for the standard Newton-Raphson method, and $\alpha_k = 1/k$ for the Robbins-Monro updates. The Robbins-Monro algorithm guarantees that the iteration prescription converges for stochastic estimations, which we use when calculating the double-bracket expectation values, as $\sum_k \alpha_k \to \infty$ while $\sum_k \alpha_k^2$ remains finite [203].

C. Ergodicity and replica exchanges

A potential ergodicity flaw of the algorithm ensues from the fact that configurations with an energy in the same interval might only be connected via local updates by allowing intermediate energies outside the interval, which is not possible within the framework defined by Eq. (11). Following Ref. [167], we apply the *replica exchange method* [204,205] to overcome this impasse. The number of replicas equals that of energy intervals used in the algorithm, $N_{\text{rep}} = N$. Furthermore, we choose the energy intervals to overlap with the neighboring ones and simulate all intervals in parallel, by fixing the central energies to be spaced by half the interval width [172,173], so that

$$E_0^{(n+1)} - E_0^{(n)} = \Delta_E/2, \quad (16)$$

and setting $\delta = \Delta_E$.

When two Markov chains of neighbor intervals are in the overlap region, we swap them with a probability of

$$P_{\text{swap}} = \min\left(1, e^{(S[A^{(n)}] - S[A^{(n+1)}])(a^{(n)} - a^{(n+1)})}\right). \quad (17)$$

We further modify Eq. (11) for the first and last energy intervals, $n = 1$ and $n = N = N_{\text{rep}}$, by allowing the Monte Carlo to probe energies outside the range $[E_{\min}, E_{\max}]$, with probability distribution proportional to the Boltzmann weight $\exp(-\beta S[A])$, as in typical importance sampling calculations. This allows the Markov chains to probe all possible energies and thus ensure ergodicity.

D. Error estimation

In our numerical calculations, we terminate the iteration in Eq. (15) after a fixed number of updating steps. We initialize the system by performing a fixed number of Newton-Raphson updates, n_{NR}. We follow this by a fixed number of Robbins-Monro updates, n_{RM} We estimate the error by repeating the same iteration prescription multiple times, while starting from a different random configuration. Error estimates are then obtained using a jackknife analysis over the final result of the repeated calculations, N_{repeats}.

III. LATTICE FORMULATION

The ensemble averages entering Eq. (14), and hence the reconstruction of the density of states, are computed by discretizing the theory on a hypercubic lattice with finite spacing, a, and space-time volume, $\tilde{V} = (N_t a) \times (N_s a)^3$. We impose periodic boundary conditions in all directions, and interpret the temporal extent of the lattice, characterized by $N_t < N_s$, in terms of the temperature of the system at equilibrium.

We adopt the Wilson gauge action, expressed in terms of the plaquette, $U_{\mu\nu}(x)$, itself a function of a (gauge) link configuration as

$$S[U] \equiv \frac{1}{N_c} \sum_x \sum_{\mu<\nu} \text{Re Tr}[1 - U_{\mu\nu}(x)]. \quad (18)$$

It is notationally convenient to express the action, $S[U]$, in terms of the average value of the plaquette

$$u_p \equiv \frac{a^4}{6\tilde{V}} \frac{1}{N_c} \sum_x \sum_{\mu<\nu} \text{Re Tr}[U_{\mu\nu}(x)], \quad (19)$$

where $N_c = 4$, for $Sp(4)$, and use the equivalent expression

$$S[U] = \frac{6\tilde{V}}{a^4}(1 - u_p[U]). \quad (20)$$

Our measurements are characterized by the extent of the lattice, the range of energies considered—equivalently, the average plaquette, u_p—the number of intervals/replica, $N = N_{\text{rep}}$, and repeats. We report the lattice sizes and parameters used in this work in Table I, in which we indicate explicitly also the number of NR and RM iterations, for each lattice. As anticipated, the HiRep code [198,199], supplemented with the symplectic adaptations [178,200], has been used, in particular for the domain decomposition of the heat bath algorithm [173,202]. We decompose each replica into four domains, along one of the spatial dimensions, as in Ref. [173]. Every double-bracket expectation value is based on a restricted Monte Carlo Markov chain. We first perform 300 updates to thermalize the energy-restricted Markov chain. We then measure the operator of interest on 700 thermalized configurations, generated using the restricted heat bath method.

A. Thermodynamics

Borrowing notation from Ref. [173], we can make use of the following identifications, that bring the system back into a form familiar from statistical mechanics. We define the entropy as

$$s \equiv \log(\rho), \quad (21)$$

noting that this definition is valid up to an additive constant—see the earlier discussion about the constant $c^{(0)}$. The energy, $E = S$, is identified with the internal energy, and hence the temperature, t, is given by

$$t \equiv \frac{\partial E}{\partial s} = \frac{1}{a^{(n)}}. \tag{22}$$

A Legendre transform yields the free energy, F, as

$$F = E - ts. \tag{23}$$

A second additive constant appears in this definition, and, following Ref. [173], we conventionally set it so that F vanishes at criticality.

Having reconstructed the density of states, and by making use of Eq. (8), we can provide a first measurement of the critical coupling, $\beta_{CV}(P)$, for a given value of N_t and N_s, by dialing β so that the probability distribution of the partition function, $P_\beta(E)$—equivalently the probability distribution of the average plaquette, $P_\beta(u_p)$, obtained by inverting Eq. (20)—displays a double Gaussian shape, with two peaks of equal height at different values of u_p.[5]

Alternative definitions of critical coupling rely on other observables. For example, we consider both the specific heat, C_V, and the Binder cumulant, B_V. Both can be expressed in terms of moments of the average plaquette, given, respectively, by

$$C_V(\beta) \equiv \frac{6V}{a^4}[\langle u_p^2\rangle_\beta - \langle u_p\rangle_\beta^2], \tag{24}$$

$$B_V(\beta) \equiv 1 - \frac{\langle u_p^4\rangle_\beta}{3\langle u_p^2\rangle_\beta^2}. \tag{25}$$

At the critical coupling, the specific heat displays a maximum, whereas the Binder cumulant exhibits a minimum. The resulting definition of $\beta_{CV}(C_V)$ and $\beta_{CV}(B_V)$ converge to the same physical temperature in the thermodynamic and continuum limit as $\beta_{CV}(P)$, hence the study of the discrepancy between them provides a useful indicator of the methodological systematics appearing in our calculations.

Assuming that the aspect ratio, N_s/N_t, is sufficiently large, we can extract the surface tension, σ_{cd}, of the bubble walls separating different phases at the confinement/deconfinement transition. Following Refs. [28,206], the interface tension is related to the minimum and maximum of the probability distribution obtained by tuning β to the critical value defined by the appearance of peaks with equal heights. One expects that the probabilities computed at the peaks and at the minimum in the valley between them scale as follows:

$$\frac{P_{\min}}{P_{\max}} \propto \sqrt{N_s}\exp\left(-2\left(\frac{N_s}{N_t}\right)^2\frac{\sigma_{cd}}{T_c^3}\right), \tag{26}$$

[5]We could as well require the appearance of two peaks with height ratio fixed to a difference conventional factor. As long as the thermodynamic limit leads to two δ functions, the same critical coupling will be recovered—see Appendix.

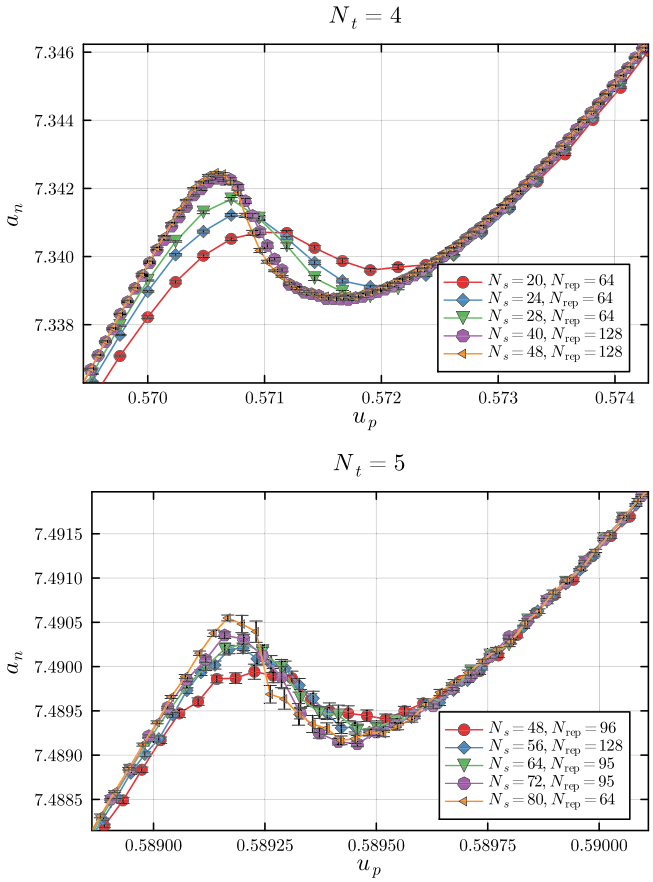

FIG. 1. Results for the coefficients, $a^{(n)}$, entering the piecewise-linear approximation of the logarithm of the density of states, as a function of the average plaquette, u_p, computed in the middle of each finite energy interval, $\Delta_E/2$. In both cases with $N_t = 4$ (top panel) and $N_t = 5$ (bottom), we show results for all available volumes. For volumes for which we performed the calculations with more than one choice of the interval size, we display only the results with the smallest Δ_E.

where T_c is the critical temperature. In our numerical data, we study the quantity [28],

$$\tilde{I} = -\frac{1}{2}\left(\frac{N_t}{N_s}\right)^2\log\left(\frac{P_{\min}}{P_{\max}}\right) + \frac{1}{4}\left(\frac{N_t}{N_s}\right)^2\log(N_s). \tag{27}$$

In the thermodynamic limit, $\lim_{N_s/N_t\to\infty}\tilde{I} = \sigma_{cd}/T_c^3$.

IV. NUMERICAL RESULTS

We show, in Fig. 1, our results for the values of the coefficients, $a^{(n)}$, entering the approximation of the density of states, as a function of the central value of the plaquette, u_p, for lattices with temporal extent $N_t = 4$ and $N_t = 5$. The former are exhibited for comparison purposes [173]. The sequence of values of $a^{(n)}$ approximates a multivalued (noninvertible) function of u_p, over a finite range of u_p. The difference between the peak and valley values of $a^{(n)}$ inside

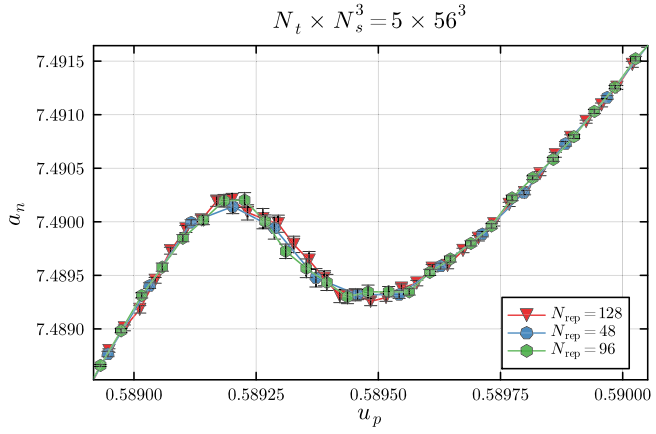

FIG. 2. Results for the coefficients, $a^{(n)}$, entering the piecewise-linear approximation of the logarithm of the density of states, as a function of the average plaquette, u_p, computed in the middle of each finite energy interval, Δ_E. Having fixed the other parameters, for the representative choice of lattice with extent $N_t \times N_s^3 = 5 \times 56^3$, we compare three different choices of number of replicas (and intervals), $N_{\rm rep}$, and hence different energy interval sizes, Δ_E. We observe no statistically significant difference between the sequences of $a^{(n)}$ obtained with these alternative choices of interval sizes.

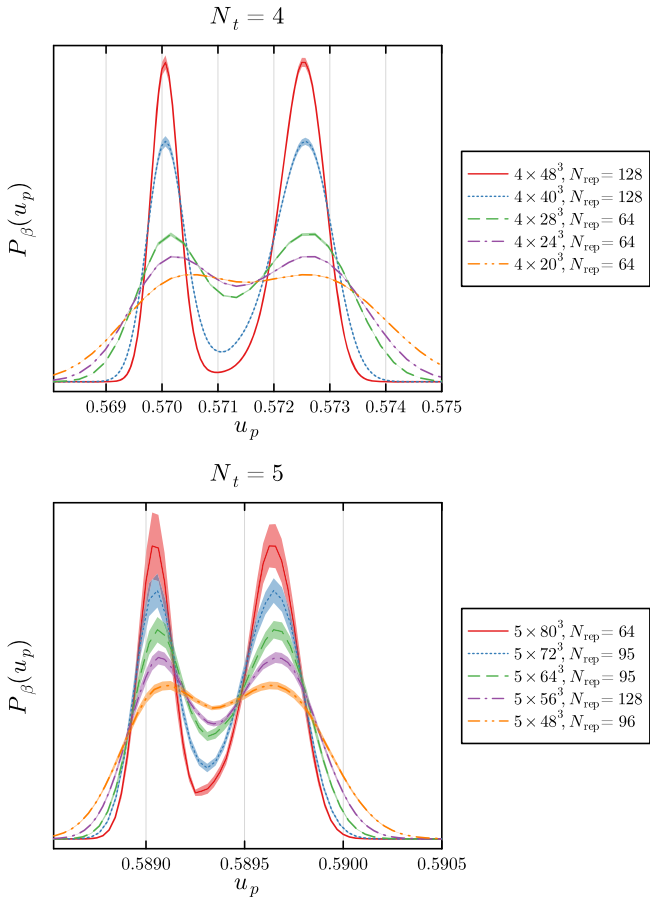

FIG. 3. Probability distribution of the plaquette, $P_\beta(u_p)$, as defined in Eq. (8), evaluated at the critical coupling, $\beta = \beta_{CV}(P)$, for $N_t = 4$ (top panel) and $N_t = 5$ (bottom panel), defined by dialing β so that the two peaks are of equal height. The probability distribution is normalized so that $\int du_p P_\beta(u_p) = 1$.

this noninvertibility range is less pronounced in the new, $N_t = 5$, measurements—roughly by a factor of three. Furthermore, the presence of a range over which $a^{(n)}$ is not invertible as a function of u_p emerges at larger values of u_p, and is restricted to a narrower range. It further emerges only at much larger aspect ratios, up to $N_s/N_t = 16$, to become clearly discernible. In existing data on $N_t = 4$ only aspect ratios up to $N_s/N_t = 12$ are available, yet the signal of metastability is clearly visible. To the best of our knowledge, the values of aspect ratios used for this publication are the largest ones deployed in published studies of this type.

In Fig. 2, we show a representative example of the comparison between the values of $a^{(n)}$ obtained with three different choices of the size of the energy intervals, $\Delta_E/2$, holding fixed the lattice parameters $N_t = 5$ and $N_s = 56$. We find good agreement between results derived with the interval sizes studied here. We take this as indication that the interval sizes used in generating the measurements presented in this paper are sufficiently small that systematic effects connected to this choice are negligible.

A common feature of Figs. 1 and 2 is that $a^{(n)}$ is not invertible as a function of u_p, yet it is unique. To verify that this is a dynamical feature, and not the product of the algorithm we use, we monitored the evolution of the NR and RM steps, and found that, for this system, independently of the starting point of the algorithm, all solutions converge to a unique value of $a^{(n)}$, for each choice of energy interval. This can be contrasted with some of the findings in the literature on holographic studies of phase transitions (see, for example Fig. 6 in Ref. [159]), which expose the possibility that, in some regions of parameter space, multiple values of the temperature (related to $a^{(n)}$) correspond to the same energy. If that were the case in realistic theories, under special conditions the out-of-equilibrium dynamics in proximity of the transition, and the process of bubble nucleation, might appear quite different from the standard paradigm, with potentially interesting implications for the generation of gravitational waves. We uncovered no evidence of such phenomena in our current measurements.

In Fig. 3, we show the (β-dependent) probability distribution of the average plaquette, $P_\beta(u_p)$, tuned to the critical coupling, $\beta = \beta_{CV}(P)$, obtained by requiring that the two peaks of the probability distribution are of equal height. The expected double-peaked structure is clearly visible, for both $N_t = 4$ and $N_t = 5$, for all available lattice volumes. In the $N_t = 5$ case, we were compelled to use substantially larger lattices and aspect ratios than in the case

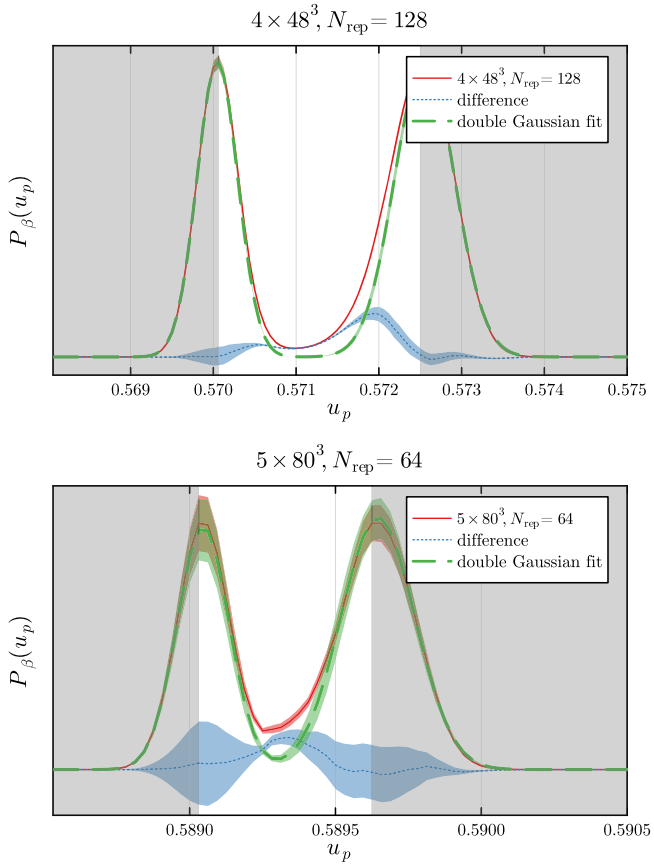

FIG. 4. Fit of the plaquette distribution, $P_\beta(u_p)$ (blue), to a bimodal Gaussian distribution (green), for the critical value of the coupling, $\beta = \beta_{CV}(P)$, and for the largest available volumes with $N_t = 4$ (top panel) and $N_t = 5$ (bottom). The gray shaded region highlights the region of the data used in the fitting procedure. We observe good agreement with the expected Gaussian behavior for large and small values of the average plaquette, while also detecting clear evidence of the effect of interfaces in the region between the peaks, as evidenced by the nonvanishing difference between measurements and fit (orange).

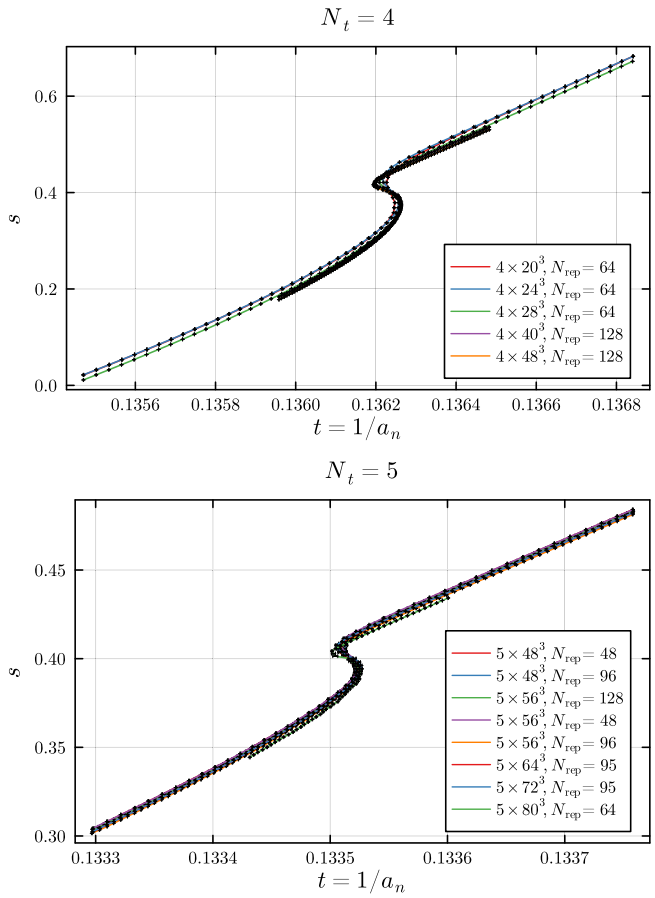

FIG. 5. Entropy, $s = \log(\rho)$, measured for $N_t = 4$ (top panel) and $N_t = 5$ (bottom), for all available calculations. We fix the unknown constant, $c^{(0)}$, in Eq. (10), and hence an additive constant in s, by requiring that the entropy is positive for all temperatures considered, and furthermore that the value of the entropy evaluated at criticality, on the unstable branch, be the same for all calculations.

of $N_t = 4$, in order to resolve this feature, and yet the separation of the peaks is less pronounced at the spatial volumes available.

In the two panels of Fig. 4, we show our measurements of $P_\beta(u_p)$ in the largest available spatial volumes, for $N_t = 4$ and $N_t = 5$, respectively. We fit the probability, $P_\beta(u_p)$, computed with $\beta = \beta_{CV}(P)$, to a bimodal Gaussian distribution. If there were no interfaces between the two phases, the plaquette distribution would be given by two Gaussians of equal height, and hence be well reproduced by the bimodal fit. This behavior assumes that there are two independent subsystems corresponding to the two phases—see the discussion in Refs. [28,173]. We exclude the energy range between the two peaks from the fit and find that our data fit nicely a Gaussian behavior, as expected in the absence of interfaces. In the central region, we clearly see the effects of an emerging interface. To help visualize this qualitative effect, the figure shows also the difference between our data and the fit. This figure provides clear evidence of a nonvanishing deviation from the Gaussian behavior in the region between the two peaks, which encodes the physics of the mixed phases. In particular, for suitably large volumes this study would allow us to measure the surface tension, as anticipated.

A. Thermodynamic properties

Within the LLR approach, we can determine the entropy only up to an additive constant, given by $c^{(0)}$ in Eq. (10). In principle, this constant should be fixed by imposing the third law of thermodynamics, but as anticipated we can only consider temperatures around the phase transition, for this work, and not the low temperatures entering the third law. We fix the unknown constant in the entropy by requiring that s be positive for all temperatures considered. Furthermore, we require that when evaluating the entropy

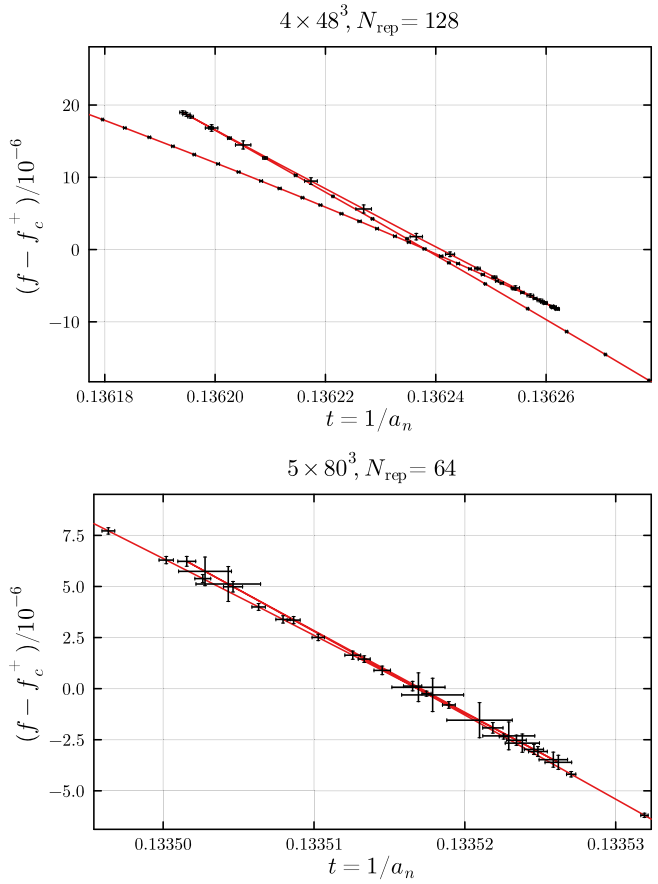

FIG. 6. Subtracted free energy density, $f-f_c^+$, determined as the Legendre transform of the internal energy, E. We fix the unknown constant in the entropy, s, by requiring that the entropy remains positive for all temperatures, and agrees across all different volumes when computed at criticality, on the unstable branch. We find the expected swallow-tail behavior.

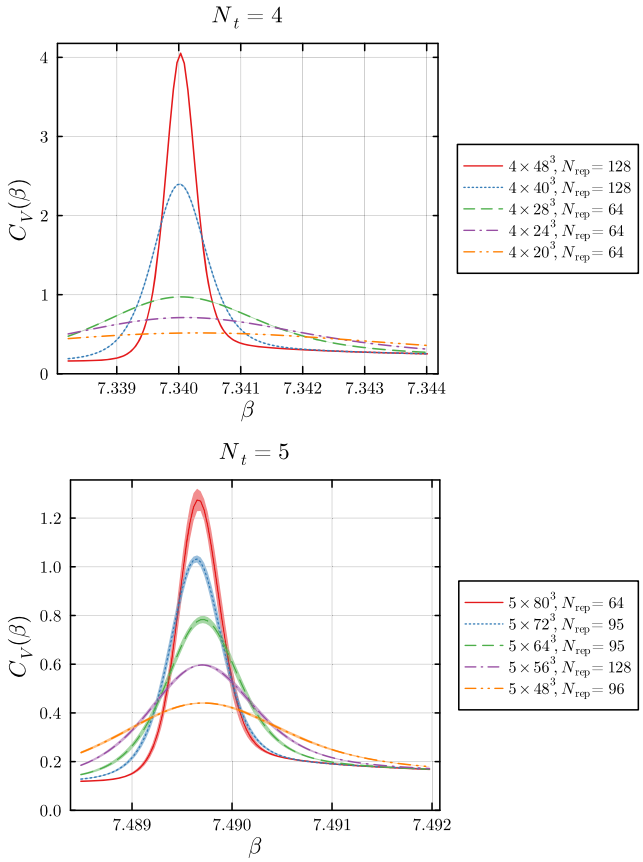

FIG. 7. Specific heat, $C_V(\beta)$, for $N_t=4$ (top panel) and $N_t=5$ (bottom). The peaks at $\beta=\beta_{CV}(C_V)$ scale as we approach the thermodynamic limit. We observe that the maximum at $N_t=5$ is lower for the same aspect ratio N_s/N_t.

at criticality, on the unstable branch in the regime of phase coexistence, we obtain the same result for all volumes studied here.

We show the entropy used in the determination of the free energy in Fig. 5. We determine the free energy as the Legendre transform of the internal energy, E, and subtract its value at the point where the two metastable branches cross. In Fig. 6, we depict the free energy density, $f=\frac{a^4}{\bar{V}}F$, as a function of the microcanonical temperature, $t=1/a_n$. We observe the appearance of the characteristic swallow-tail shape that accompanies the phenomena of phase coexistence and metastability. If we were able to probe the system at lower temperatures and fix the unknown constant, in Eq. (23), through the third law of thermodynamics, $\lim_{t\to 0} s=0$, the slope of the free energy would be expected to be steeper.

As a further consistency check, and to assess the size of methodological systematics, we also determine the critical coupling in two more conventional ways, by examining the specific heat [which has a maximum at $\beta=\beta_{CV}(C_V)$], and the Binder cumulant [which has a minimum at $\beta=\beta_{CV}(B_V)$], using Eqs. (24) and (25). We show the specific heat around the critical coupling in Fig. 7, and the Binder cumulant in Fig. 8.

We determine the critical coupling, $\beta_{CV}(C_V)$ [$\beta_{CV}(B_V)$], by identifying the maximum (minimum) of the respective cumulant. We show the numerical values of β_{CV} obtained at different lattice volumes and using different observables in Table II and Fig. 9. For the measurements with $N_t=4$, these results have already been published in Ref. [173], and we observe the presence of statistically significant deviations between the determinations arising from the probability distribution and the specific heat as well as the Binder cumulant. We do not observe such an effect for our new measurements at $N_t=5$ within current uncertainties.

In Fig. 10, we plot $\tilde{I}$, computed according to Eq. (27), for all available ensembles, including both the cases of $N_t=4$ and $N_t=5$. We find that the term $\tilde{I}$ is strongly suppressed for $N_t=5$, in comparison to $N_t=4$, for all available choices of aspect ratio, N_t/N_s, and hence that this quantity is, with current lattices, affected by large lattice artifacts. It is likely that finer lattices at $N_t\geq 6$ are required to perform

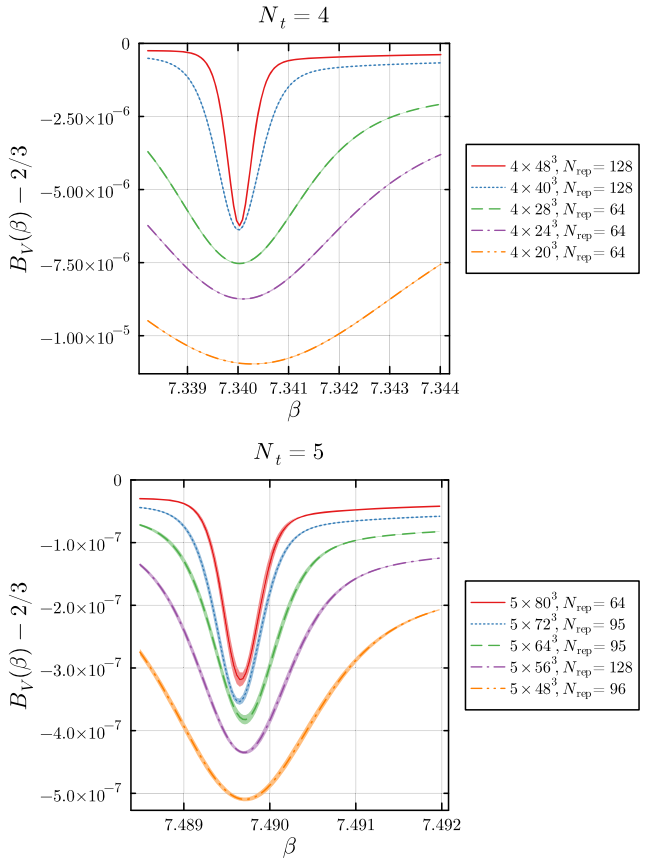

FIG. 8. Deviation of the Binder cumulant from two thirds, $B_V(\beta) - 2/3$, for $N_t = 4$ (top panel) and $N_t = 5$ (bottom). We observe a minimum at the critical coupling $\beta_{CV}(B_V)$.

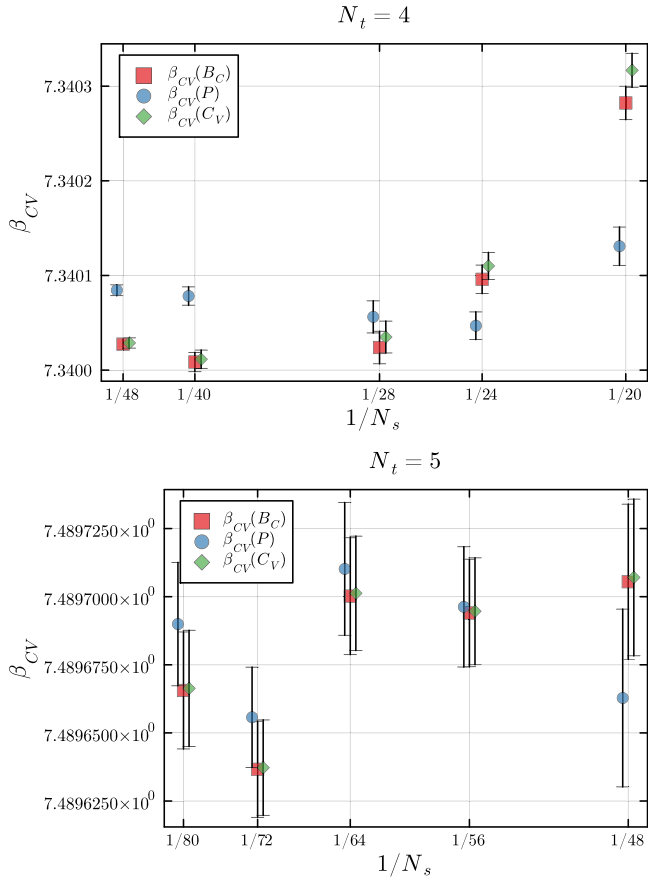

FIG. 9. Plot of the data presented in Table II. For comparison, we show the critical couplings for both $N_t = 4$, which were first presented in Ref. [173], and $N_t = 5$, original to this work.

TABLE II. Three complementary determinations of the critical coupling of the $Sp(4)$ Yang-Mills theory, obtained from different observables: the plaquette distribution, $P_\beta(u_p)$, the specific heat, $C_V(\beta)$, and the Binder cumulant, $B_V(\beta)$. We report our best measurements for all available lattices. For comparison, we report both results for $N_t = 4$, which were first presented in Ref. [173], and $N_t = 5$, original to this work.

N_t	N_s	$N_{\rm rep}$	$\beta_{CV}(P)$	$\beta_{CV}(C_V)$	$\beta_{CV}(B_V)$
5	48	48	7.489685(36)	7.489735(34)	7.489733(34)
5	48	96	7.489663(33)	7.489707(29)	7.489705(28)
5	56	128	7.489696(22)	7.489695(20)	7.489694(20)
5	56	48	7.489678(32)	7.489679(29)	7.489680(30)
5	56	96	7.489678(25)	7.489680(24)	7.489681(24)
5	64	95	7.489710(24)	7.489701(21)	7.489700(21)
5	72	95	7.489656(18)	7.489637(18)	7.489637(18)
5	80	64	7.489690(23)	7.489666(21)	7.489666(21)
4	20	64	7.340131(20)	7.340317(18)	7.340282(18)
4	24	64	7.340047(15)	7.340110(14)	7.340096(15)
4	28	64	7.340056(17)	7.340035(17)	7.340024(17)
4	40	128	7.3400783(97)	7.3400115(97)	7.340009(10)
4	48	128	7.3400844(57)	7.3400287(54)	7.3400275(54)

the full continuum limit. Nevertheless, the very fact that we could extract this quantity brings our current understanding of the surface tensions in the $Sp(4)$ Yang-Mills theory close to the state of the art for other theories, in particular those with $SU(N_c)$ gauge group—see, e.g., Refs. [28,207,208]

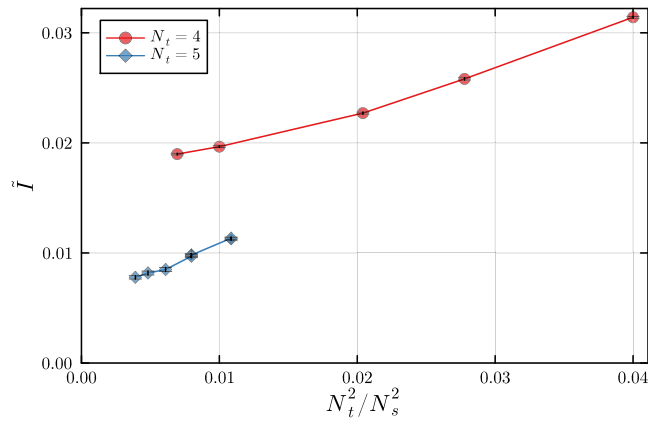

FIG. 10. Our numerical results for the term, $\tilde{I}$, giving rise to the dimensionless surface tension, σ_{cd}/T_c^3, in the limit of vanishing inverse aspect ratio, $N_t/N_s \to 0$, for all available lattices.

and references therein, in particular Refs. [209–211]. Our results for $\hat{I}$ are roughly of the same size as for $SU(3)$ [28,209–211] suggesting that the transition in $Sp(4)$ is a weak first-order transition.

V. CONCLUSION AND OUTLOOK

We presented our results for a new set of lattice studies of the finite-temperature, confinement-deconfinement phase transition in the $Sp(4)$ Yang-Mills theory. Using the LLR algorithm to implement the density of states framework, we made the first steps toward the continuum limit extrapolation, by providing an extensive set of results for lattices with temporal extent $N_t = 5$, that complement earlier measurements for $N_t = 4$. Our calculations have been performed for several choices of (large) spatial volumes, so that the thermodynamic (infinite-volume) limit can be approached. We have further shown that for our choices of finite discretization of the energy, systematic effects arising from the LLR implementation are negligible.

We demonstrated that we can resolve a first-order phase transition effectively with the LLR method on fine lattices.

We have used significantly larger lattice volumes than has been done in past investigations within Yang-Mills theories. We found that larger aspect ratios were required to resolve the phase transition. We estimated the critical coupling for finite volumes, β_{CV}, through several independent prescriptions and found that the measurements are robust, being compatible with one another.

In contrast to existing results for $N_t = 4$, in the case of $N_t = 5$ this analysis suggests that the error budget is dominated by the statistical uncertainties in a_n, rather than by methodological systematics.

We provided a first quantitative assessment of the size of discretization artifacts present in the determination of the surface tension. The current measurement of the surface tension sets an upper limit on its true value, that is important as input into realistic estimates of the GW power spectrum of the continuum theory. This study provides numerical evidence for the need to deploy even larger lattices, in order to approach the continuum limit and provide a high precision measurement of this quantity.

Further progress is achievable in future studies, by considering finer lattices, and hence larger values of N_t. Doing so will require considering larger aspect ratios, N_s/N_t, which will increase the cost of the calculations, and demand further algorithm and software development for the implementation of the global constraint on the internal energy underpinning the LLR algorithm, in order to optimize the parallelization of the underlying calculation.

The workflow used to analyse these data is available at Ref. [212]. The modified HiRep code with support for the LLR is available at [202]. It is based upon [199,200].

ACKNOWLEDGMENTS

We would like to thank Stephan J. Huber, David Mateos, and Manuel Reichert for useful discussions, and Frederic D. R. Bonnet for help in benchmarking our code. The work of E. B. and B. L. is supported in part by the EPSRC ExCALIBUR program ExaTEPP (Project No. EP/X017168/1). The work of E. B. has also been supported by the UKRI Science and Technology Facilities Council (STFC) Research Software Engineering Fellowship EP/V052489/1. The work of E. B., B. L., and M. P. has been supported in part by the STFC Consolidated Grant No. ST/X000648/1. The work of B. L. is supported in part by the STFC Consolidator Grant No. ST/X00063X/1. The work of B. L. and M. P. has been supported in part by the STFC Consolidated Grant No. ST/T000813/1. B. L. and M. P. received funding from the European Research Council (ERC) under the European Union's Horizon 2020 research and innovation program under Grant Agreement No. 813942. D. M. has been supported in part by a studentship awarded by the Data Intensive Centre for Doctoral Training, funded by the STFC Grant No. ST/P006779/1. D. V. is supported in part by STFC under Consolidated Grant No. ST/X000680/1. F. Z. is supported by the STFC Consolidated Grant No. ST/X000648/1. This work used the DiRAC Data Intensive service (CSD3) at the University of Cambridge, the DiRAC Data Intensive service (DIaL3) at the University of Leicester and the DiRAC Extreme Scaling service (Tursa) at the University of Edinburgh, managed respectively by the University of Cambridge University Information Services, the University of Leicester Research Computing Service and by EPCC on behalf of the STFC DiRAC HPC Facility [213]. The DiRAC service at Cambridge, Leicester, and Edinburgh are funded by BEIS, UKRI and STFC capital funding and STFC operations grants. DiRAC is part of the UKRI Digital Research Infrastructure. This work was supported by the Supercomputer Fugaku Start-up Utilization Program of RIKEN. This work used computational resources of the supercomputer Fugaku provided by RIKEN through the HPCI System Research Project (Project No. hp230397). Numerical simulations have been performed on the Swansea SUNBIRD cluster (part of the Supercomputing Wales project). The Swansea SUNBIRD system is part funded by the European Regional Development Fund (ERDF) via the Welsh Government.

DATA AVAILABILITY

The data that support the findings of this article are openly available [214].

APPENDIX: MORE ON DETERMINING $\beta_{CV}(P)$

In Sec. IV, we provided a determination of the critical coupling, $\beta_{CV}(P)$, obtained by requiring that the

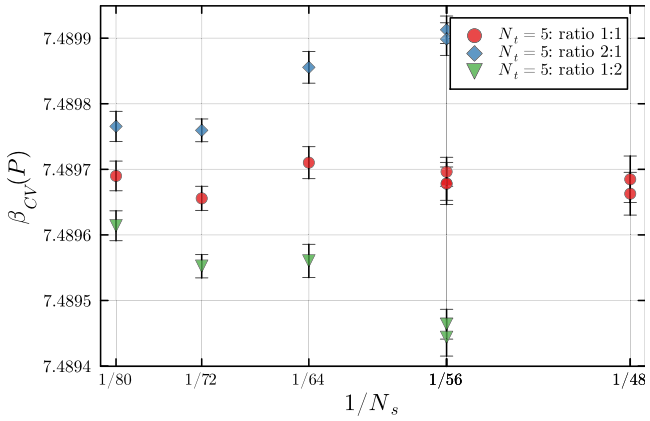

FIG. 11. Critical $\beta_{CV}(P)$ as determined (at finite volume) by analysis $P_\beta(u_p)$, and dialing β to different ratios of peak heights in the plaquette distribution: equal heights (yellow circles) and peak-height-ratio of two to one (blue hexagons) and one to two (green rectangles).

probability distribution of the plaquette, $P_\beta(u_p)$, displays two peaks of equal heights. In this Appendix we consider a modified prescription, in which we require that one of the peaks is twice the height of the other. In part, this is motivated by the suggestion that, in the presence of multiple choices of vacuum in the one of the phases, one might require that such multiplicity be taken into account [215]. We hence examine how the resulting measurements of $\beta_{CV}(P)$, emerging from these three alternative prescriptions, approach the infinite volume limit.

We show the results of this analysis in Fig. 11. Finite volume corrections are much more pronounced in the case of prescriptions based on tuning $P_\beta(u_p)$ to display peaks with unequal heights. Thus, in the main body of the paper, we restrict ourselves to the definition of $\beta_{CV}(P)$ adopted in from Sec. IV.

[1] S. Borsanyi, K. R., Z. Fodor, D. A. Godzieba, P. Parotto, and D. Sexty, Precision study of the continuum $SU(3)$ Yang-Mills theory: How to use parallel tempering to improve on supercritical slowing down for first order phase transitions, Phys. Rev. D **105**, 074513 (2022).

[2] G. Aarts *et al.*, Phase transitions in particle physics—results and perspectives from lattice quantum chromodynamics, Prog. Part. Nucl. Phys. **133**, 104070 (2023).

[3] B. Svetitsky and L. G. Yaffe, Critical behavior at finite temperature confinement transitions, Nucl. Phys. **B210**, 423 (1982).

[4] L. G. Yaffe and B. Svetitsky, First order phase transition in the $SU(3)$ gauge theory at finite temperature, Phys. Rev. D **26**, 963 (1982).

[5] K. Kajantie, C. Montonen, and E. Pietarinen, Phase transition of $SU(3)$ gauge theory at finite temperature, Z. Phys. C **9**, 253 (1981).

[6] T. Celik, J. Engels, and H. Satz, The order of the deconfinement transition in $SU(3)$ Yang-Mills theory, Phys. Lett. B **125**, 411 (1983).

[7] J. B. Kogut, H. Matsuoka, M. Stone, H. W. Wyld, S. H. Shenker, J. Shigemitsu, and D. K. Sinclair, Quark and gluon latent heats at the deconfinement phase transition in $SU(3)$ gauge theory, Phys. Rev. Lett. **51**, 869 (1983).

[8] B. Svetitsky and F. Fucito, Latent heat of the $SU(3)$ gauge theory, Phys. Lett. **131B**, 165 (1983).

[9] S. A. Gottlieb, J. Kuti, D. Toussaint, A. D. Kennedy, S. Meyer, B. J. Pendleton, and R. L. Sugar, The deconfining phase transition and the continuum limit of lattice quantum chromodynamics, Phys. Rev. Lett. **55**, 1958 (1985).

[10] F. R. Brown, N. H. Christ, Y. F. Deng, M. S. Gao, and T. J. Woch, Nature of the deconfining phase transition in $SU(3)$ lattice gauge theory, Phys. Rev. Lett. **61**, 2058 (1988).

[11] M. Fukugita, M. Okawa, and A. Ukawa, Order of the deconfining phase transition in $SU(3)$ lattice gauge theory, Phys. Rev. Lett. **63**, 1768 (1989).

[12] P. Bacilieri *et al.*, A new computation of the correlation length near the deconfining transition in $SU(3)$, Phys. Lett. B **224**, 333 (1989).

[13] N. A. Alves, B. A. Berg, and S. Sanielevici, Binder energy cumulant for $SU(3)$ lattice gauge theory, Phys. Lett. B **241**, 557 (1990).

[14] G. Boyd, J. Engels, F. Karsch, E. Laermann, C. Legeland, M. Lutgemeier, and B. Petersson, Equation of state for the $SU(3)$ gauge theory, Phys. Rev. Lett. **75**, 4169 (1995).

[15] G. Boyd, J. Engels, F. Karsch, E. Laermann, C. Legeland, M. Lutgemeier, and B. Petersson, Thermodynamics of $SU(3)$ lattice gauge theory, Nucl. Phys. **B469**, 419 (1996).

[16] S. Borsanyi, G. Endrodi, Z. Fodor, S. D. Katz, and K. K. Szabo, Precision $SU(3)$ lattice thermodynamics for a large temperature range, J. High Energy Phys. 07 (2012) 056.

[17] M. Shirogane, S. Ejiri, R. Iwami, K. Kanaya, and M. Kitazawa, Latent heat at the first order phase transition point of $SU(3)$ gauge theory, Phys. Rev. D **94**, 014506 (2016).

[18] WHOT-QCD Collaboration, Phase structure of finite temperature QCD in the heavy quark region, Phys. Rev. D **84**, 054502 (2011).

[19] WHOT-QCD Collaboration, End point of the first-order phase transition of QCD in the heavy quark region by reweighting from quenched QCD, Phys. Rev. D **101**, 054505 (2020).

[20] A. Kiyohara, M. Kitazawa, S. Ejiri, and K. Kanaya, Finite-size scaling around the critical point in the heavy quark region of QCD, Phys. Rev. D **104**, 114509 (2021).

[21] M. Fromm, J. Langelage, S. Lottini, and O. Philipsen, The QCD deconfinement transition for heavy quarks and all baryon chemical potentials, J. High Energy Phys. 01 (2012) 042.

[22] F. Cuteri, O. Philipsen, A. Schön, and A. Sciarra, Deconfinement critical point of lattice QCD with $N_f = 2$ Wilson fermions, Phys. Rev. D **103**, 014513 (2021).

[23] L. Dini, P. Hegde, F. Karsch, A. Lahiri, C. Schmidt, and S. Sharma, Chiral phase transition in three-flavor QCD from lattice QCD, Phys. Rev. D **105**, 034510 (2022).

[24] S. Borsanyi, Z. Fodor, J. N. Guenther, R. Kara, P. Parotto, A. Pasztor *et al.*, The upper right corner of the columbia plot with staggered fermions, Proc. Sci. LATTICE2021 (**2022**) 496 [arXiv:2112.04192].

[25] B. Lucini, M. Teper, and U. Wenger, The deconfinement transition in $SU(N)$ gauge theories, Phys. Lett. B **545**, 197 (2002).

[26] B. Lucini, M. Teper, and U. Wenger, The high temperature phase transition in $SU(N)$ gauge theories, J. High Energy Phys. 01 (2004) 061.

[27] K. Holland, M. Pepe, and U. J. Wiese, The deconfinement phase transition of Sp(2) and Sp(3) Yang-Mills theories in $(2+1)$-dimensions and $(3+1)$-dimensions, Nucl. Phys. **B694**, 35 (2004).

[28] B. Lucini, M. Teper, and U. Wenger, Properties of the deconfining phase transition in $SU(N)$ gauge theories, J. High Energy Phys. 02 (2005) 033.

[29] M. Pepe, Confinement and the center of the gauge group, Proc. Sci. LAT2005 (**2006**) 017 [arXiv:hep-lat/0510013].

[30] M. Pepe and U. J. Wiese, Exceptional deconfinement in G_2 gauge theory, Nucl. Phys. **B768**, 21 (2007).

[31] G. Cossu, M. D'Elia, A. Di Giacomo, B. Lucini, and C. Pica, G_2 gauge theory at finite temperature, J. High Energy Phys. 10 (2007) 100.

[32] M. Panero, Thermodynamics of the QCD plasma and the large-N limit, Phys. Rev. Lett. **103**, 232001 (2009).

[33] S. Datta and S. Gupta, Continuum thermodynamics of the GluoN_c plasma, Phys. Rev. D **82**, 114505 (2010).

[34] B. Lucini, A. Rago, and E. Rinaldi, $SU(N_c)$ gauge theories at deconfinement, Phys. Lett. B **712**, 279 (2012).

[35] M. Bruno, M. Caselle, M. Panero, and R. Pellegrini, Exceptional thermodynamics: The equation of state of G_2 gauge theory, J. High Energy Phys. 03 (2015) 057.

[36] T. Appelquist *et al.*, Stealth dark matter: Dark scalar baryons through the Higgs portal, Phys. Rev. D **92**, 075030 (2015).

[37] T. Appelquist *et al.*, Detecting stealth dark matter directly through electromagnetic polarizability, Phys. Rev. Lett. **115**, 171803 (2015).

[38] Lattice Strong Dynamics Collaboration, Stealth dark matter confinement transition and gravitational waves, Phys. Rev. D **103**, 014505 (2021).

[39] M. Bruno, N. Forzano, M. Panero, and A. Smecca, Thermal evolution of dark matter in the early universe from a symplectic glueball model, J. Cosmol. Astropart. Phys. 01 (2026) 049.

[40] M. J. Strassler and K. M. Zurek, Echoes of a hidden valley at hadron colliders, Phys. Lett. B **651**, 374 (2007).

[41] K. Cheung and T.-C. Yuan, Hidden fermion as milli-charged dark matter in Stueckelberg Z- prime model, J. High Energy Phys. 03 (2007) 120.

[42] T. Hambye, Hidden vector dark matter, J. High Energy Phys. 01 (2009) 028.

[43] J. L. Feng, M. Kaplinghat, H. Tu, and H.-B. Yu, Hidden charged dark matter, J. Cosmol. Astropart. Phys. 07 (2009) 004.

[44] T. Cohen, D. J. Phalen, A. Pierce, and K. M. Zurek, Asymmetric dark matter from a GeV hidden sector, Phys. Rev. D **82**, 056001 (2010).

[45] R. Foot and S. Vagnozzi, Dissipative hidden sector dark matter, Phys. Rev. D **91**, 023512 (2015).

[46] G. Bertone and D. Hooper, History of dark matter, Rev. Mod. Phys. **90**, 045002 (2018).

[47] E. Del Nobile, C. Kouvaris, and F. Sannino, Interfering composite asymmetric dark matter for DAMA and CoGeNT, Phys. Rev. D **84**, 027301 (2011).

[48] A. Hietanen, R. Lewis, C. Pica, and F. Sannino, Composite Goldstone dark matter: Experimental predictions from the lattice, J. High Energy Phys. 12 (2014) 130.

[49] J. M. Cline, W. Huang, and G. D. Moore, Challenges for models with composite states, Phys. Rev. D **94**, 055029 (2016).

[50] G. Cacciapaglia, C. Pica, and F. Sannino, Fundamental composite dynamics: A review, Phys. Rep. **877**, 1 (2020).

[51] N. A. Dondi, F. Sannino, and J. Smirnov, Thermal history of composite dark matter, Phys. Rev. D **101**, 103010 (2020).

[52] S. Ge, K. Lawson, and A. Zhitnitsky, Axion quark nugget dark matter model: Size distribution and survival pattern, Phys. Rev. D **99**, 116017 (2019).

[53] V. Beylin, M. Y. Khlopov, V. Kuksa, and N. Volchanskiy, Hadronic and hadron-like physics of dark matter, Symmetry **11**, 587 (2019).

[54] N. Yamanaka, H. Iida, A. Nakamura, and M. Wakayama, Dark matter scattering cross section and dynamics in dark Yang-Mills theory, Phys. Lett. B **813**, 136056 (2021).

[55] N. Yamanaka, H. Iida, A. Nakamura, and M. Wakayama, Glueball scattering cross section in lattice SU(2) Yang-Mills theory, Phys. Rev. D **102**, 054507 (2020).

[56] H. Cai and G. Cacciapaglia, Singlet dark matter in the SU(6)/SO(6) composite Higgs model, Phys. Rev. D **103**, 055002 (2021).

[57] Y. Hochberg, E. Kuflik, T. Volansky, and J. G. Wacker, Mechanism for thermal relic dark matter of strongly interacting massive particles, Phys. Rev. Lett. **113**, 171301 (2014).

[58] Y. Hochberg, E. Kuflik, H. Murayama, T. Volansky, and J. G. Wacker, Model for thermal relic dark matter of strongly interacting massive particles, Phys. Rev. Lett. **115**, 021301 (2015).

[59] Y. Hochberg, E. Kuflik, and H. Murayama, SIMP spectroscopy, J. High Energy Phys. 05 (2016) 090.

[60] N. Bernal, X. Chu, and J. Pradler, Simply split strongly interacting massive particles, Phys. Rev. D **95**, 115023 (2017).

[61] A. Berlin, N. Blinov, S. Gori, P. Schuster, and N. Toro, Cosmology and accelerator tests of strongly interacting dark matter, Phys. Rev. D **97**, 055033 (2018).

[62] N. Bernal, X. Chu, S. Kulkarni, and J. Pradler, Self-interacting dark matter without prejudice, Phys. Rev. D **101**, 055044 (2020).

[63] Y.-D. Tsai, R. McGehee, and H. Murayama, Resonant Self-Interacting dark matter from dark QCD, Phys. Rev. Lett. **128**, 172001 (2022).

[64] D. Kondo, R. McGehee, T. Melia, and H. Murayama, Linear sigma dark matter, J. High Energy Phys. 09 (2022) 041.

[65] X. Chu, M. Nikolic, and J. Pradler, Even SIMP miracles are possible, Phys. Rev. Lett. **133**, 021003 (2024).

[66] A. Maas and F. Zierler, Strong isospin breaking in $\boldsymbol{Sp}(4)$ gauge theory, Proc. Sci. LATTICE2021 (**2022**) 130 [arXiv:2109.14377].

[67] F. Zierler and A. Maas, $Sp(4)$ SIMP dark matter on the lattice, Proc. Sci.LHCP2021 (**2021**) 162.

[68] S. Kulkarni, A. Maas, S. Mee, M. Nikolic, J. Pradler, and F. Zierler, Low-energy effective description of dark $Sp(4)$ theories, SciPost Phys. **14**, 044 (2023).

[69] J. Pomper and S. Kulkarni, Low energy effective theories of composite dark matter with real representations, arXiv:2402.04176.

[70] G. Cacciapaglia, D. Y. Cheong, A. Deandrea, W. Isnard, and S. C. Park, Composite hybrid inflation: Dilaton and waterfall pions, J. Cosmol. Astropart. Phys. 10 (2023) 063.

[71] S. Ferrante, A. Ismail, S. J. Lee, and Y. Lee, Forbidden conformal dark matter at a GeV, J. High Energy Phys. 11 (2023) 186.

[72] T. Appelquist, J. Ingoldby, and M. Piai, Dilaton forbidden dark matter, Phys. Rev. D **110**, 035013 (2024).

[73] M. Cirelli, A. Strumia, and J. Zupan, Dark matter, arXiv:2406.01705.

[74] M. Laine and K. Rummukainen, What's new with the electroweak phase transition?, Nucl. Phys. B, Proc. Suppl. **73**, 180 (1999).

[75] D. E. Morrissey and M. J. Ramsey-Musolf, Electroweak baryogenesis, New J. Phys. **14**, 125003 (2012).

[76] K. Kajantie, M. Laine, K. Rummukainen, and M. E. Shaposhnikov, Is there a hot electroweak phase transition at $m_H \gtrsim m_W$?, Phys. Rev. Lett. **77**, 2887 (1996).

[77] F. Karsch, T. Neuhaus, A. Patkos, and J. Rank, Critical Higgs mass and temperature dependence of gauge boson masses in the SU(2) gauge Higgs model, Nucl. Phys. B, Proc. Suppl. **53**, 623 (1997).

[78] M. Gurtler, E.-M. Ilgenfritz, and A. Schiller, Where the electroweak phase transition ends, Phys. Rev. D **56**, 3888 (1997).

[79] K. Rummukainen, M. Tsypin, K. Kajantie, M. Laine, and M. E. Shaposhnikov, The universality class of the electroweak theory, Nucl. Phys. **B532**, 283 (1998).

[80] F. Csikor, Z. Fodor, and J. Heitger, Endpoint of the hot electroweak phase transition, Phys. Rev. Lett. **82**, 21 (1999).

[81] Y. Aoki, F. Csikor, Z. Fodor, and A. Ukawa, The Endpoint of the first order phase transition of the SU(2) gauge Higgs model on a four-dimensional isotropic lattice, Phys. Rev. D **60**, 013001 (1999).

[82] M. D'Onofrio and K. Rummukainen, Standard model cross-over on the lattice, Phys. Rev. D **93**, 025003 (2016).

[83] O. Gould, S. Güyer, and K. Rummukainen, First-order electroweak phase transitions: A nonperturbative update, Phys. Rev. D **106**, 114507 (2022).

[84] A. D. Sakharov, Violation of *CP* invariance, C asymmetry, and baryon asymmetry of the universe, Pis'ma Zh. Eksp. Teor. Fiz. **5**, 32 (1967).

[85] E. Witten, Cosmic separation of phases, Phys. Rev. D **30**, 272 (1984).

[86] M. Kamionkowski, A. Kosowsky, and M. S. Turner, Gravitational radiation from first order phase transitions, Phys. Rev. D **49**, 2837 (1994).

[87] B. Allen, The stochastic gravity wave background: Sources and detection, in Les Houches School of Physics: Astrophysical Sources of Gravitational Radiation (1996), **4**, pp. 373–417, arXiv:gr-qc/9604033.

[88] P. Schwaller, Gravitational waves from a dark phase transition, Phys. Rev. Lett. **115**, 181101 (2015).

[89] D. Croon, V. Sanz, and G. White, Model discrimination in gravitational wave spectra from dark phase transitions, J. High Energy Phys. 08 (2018) 203.

[90] N. Christensen, Stochastic gravitational wave backgrounds, Rep. Prog. Phys. **82**, 016903 (2019).

[91] N. Seto, S. Kawamura, and T. Nakamura, Possibility of direct measurement of the acceleration of the universe using 0.1-Hz band laser interferometer gravitational wave antenna in space, Phys. Rev. Lett. **87**, 221103 (2001).

[92] S. Kawamura *et al.*, The japanese space gravitational wave antenna DECIGO, Classical Quantum Gravity **23**, S125 (2006).

[93] J. Crowder and N. J. Cornish, Beyond LISA: Exploring future gravitational wave missions, Phys. Rev. D **72**, 083005 (2005).

[94] V. Corbin and N. J. Cornish, Detecting the cosmic gravitational wave background with the big bang observer, Classical Quantum Gravity **23**, 2435 (2006).

[95] G. M. Harry, P. Fritschel, D. A. Shaddock, W. Folkner, and E. S. Phinney, Laser interferometry for the big bang observer, Classical Quantum Gravity **23**, 4887 (2006).

[96] S. Hild *et al.*, Sensitivity studies for third-generation gravitational wave observatories, Classical Quantum Gravity **28**, 094013 (2011).

[97] K. Yagi and N. Seto, Detector configuration of DECIGO/BBO and identification of cosmological neutron-star binaries, Phys. Rev. D **83**, 044011 (2011).

[98] B. Sathyaprakash *et al.*, Scientific objectives of Einstein telescope, Classical Quantum Gravity **29**, 124013 (2012).

[99] E. Thrane and J. D. Romano, Sensitivity curves for searches for gravitational-wave backgrounds, Phys. Rev. D **88**, 124032 (2013).

[100] C. Caprini *et al.*, Science with the space-based interferometer eLISA. II: Gravitational waves from cosmological phase transitions, J. Cosmol. Astropart. Phys. 04 (2016) 001.

[101] LISA Collaboration, Laser interferometer space antenna, arXiv:1702.00786.

[102] LIGO Scientific Collaboration, Exploring the sensitivity of next generation gravitational wave detectors, Classical Quantum Gravity **34**, 044001 (2017).

[103] S. Isoyama, H. Nakano, and T. Nakamura, Multiband gravitational-wave astronomy: Observing binary inspirals with a decihertz detector, B-DECIGO, Prog. Theor. Exp. Phys. **2018**, 073E01 (2018).

[104] J. Baker *et al.*, The laser interferometer space antenna: Unveiling the millihertz gravitational wave sky, arXiv:1907.06482.
[105] V. Brdar, A. J. Helmboldt, and J. Kubo, Gravitational waves from first-order phase transitions: LIGO as a window to unexplored seesaw scales, J. Cosmol. Astropart. Phys. 02 (2019) 021.
[106] D. Reitze *et al.*, Cosmic explorer: The U.S. Contribution to gravitational-wave astronomy beyond LIGO, Bull. Am. Astron. Soc. **51**, 035 (2019).
[107] C. Caprini *et al.*, Detecting gravitational waves from cosmological phase transitions with LISA: An update, J. Cosmol. Astropart. Phys. 03 (2020) 024.
[108] M. Maggiore *et al.*, Science case for the Einstein telescope, J. Cosmol. Astropart. Phys. 03 (2020) 050.
[109] A. Afzal, G. Agazie, A. Anumarlapudi, A. M. Archibald, Z. Arzoumanian, P. T. Baker *et al.*, The NANOGrav 15 yr data set: Search for signals from new physics, Astrophys. J. Lett. **951**, L11 (2023).
[110] V. I. Kalikmanov, *Nucleation Theory*, Lecture Notes in Physics, Vol. 860 (SpringerScience+Business Media, Dordrecht, NL, 2013).
[111] B. A. Berg and T. Neuhaus, Multicanonical algorithms for first order phase transitions, Phys. Lett. B **267**, 249 (1991).
[112] W.-C. Huang, M. Reichert, F. Sannino, and Z.-W. Wang, Testing the dark $SU(N)$ Yang-Mills theory confined landscape: From the lattice to gravitational waves, Phys. Rev. D **104**, 035005 (2021).
[113] J. Halverson, C. Long, A. Maiti, B. Nelson, and G. Salinas, Gravitational waves from dark Yang-Mills sectors, J. High Energy Phys. 05 (2021) 154.
[114] Z. Kang, J. Zhu, and S. Matsuzaki, Dark confinement-deconfinement phase transition: A roadmap from Polyakov loop models to gravitational waves, J. High Energy Phys. 09 (2021) 060.
[115] M. Reichert, F. Sannino, Z.-W. Wang, and C. Zhang, Dark confinement and chiral phase transitions: Gravitational waves vs matter representations, J. High Energy Phys. 01 (2022) 003.
[116] M. Reichert and Z.-W. Wang, Gravitational waves from dark composite dynamics, EPJ Web Conf. **274**, 08003 (2022).
[117] R. Pasechnik, M. Reichert, F. Sannino, and Z.-W. Wang, Gravitational waves from composite dark sectors, J. High Energy Phys. 02 (2024) 159.
[118] R. D. Pisarski, Quark gluon plasma as a condensate of $SU(3)$ Wilson lines, Phys. Rev. D **62**, 111501 (2000).
[119] R. D. Pisarski, Tests of the Polyakov loops model, Nucl. Phys. **A702**, 151 (2002).
[120] R. D. Pisarski, Notes on the deconfining phase transition, in *Cargese Summer School on QCD Perspectives on Hot and Dense Matter* (2002), 3, pp. 353–384, arXiv:hep-ph/0203271.
[121] F. Sannino, Polyakov loops versus hadronic states, Phys. Rev. D **66**, 034013 (2002).
[122] C. Ratti, M. A. Thaler, and W. Weise, Phases of QCD: Lattice thermodynamics and a field theoretical model, Phys. Rev. D **73**, 014019 (2006).
[123] K. Fukushima and C. Sasaki, The phase diagram of nuclear and quark matter at high baryon density, Prog. Part. Nucl. Phys. **72**, 99 (2013).
[124] K. Fukushima and V. Skokov, Polyakov loop modeling for hot QCD, Prog. Part. Nucl. Phys. **96**, 154 (2017).
[125] P. M. Lo, B. Friman, O. Kaczmarek, K. Redlich, and C. Sasaki, Polyakov loop fluctuations in $SU(3)$ lattice gauge theory and an effective gluon potential, Phys. Rev. D **88**, 074502 (2013).
[126] H. Hansen, R. Stiele, and P. Costa, Quark and Polyakov-loop correlations in effective models at zero and non-vanishing density, Phys. Rev. D **101**, 094001 (2020).
[127] P. N. Meisinger, T. R. Miller, and M. C. Ogilvie, Phenomenological equations of state for the quark gluon plasma, Phys. Rev. D **65**, 034009 (2002).
[128] A. Dumitru, Y. Guo, Y. Hidaka, C. P. K. Altes, and R. D. Pisarski, How wide is the transition to deconfinement?, Phys. Rev. D **83**, 034022 (2011).
[129] A. Dumitru, Y. Guo, Y. Hidaka, C. P. K. Altes, and R. D. Pisarski, Effective matrix model for deconfinement in pure gauge theories, Phys. Rev. D **86**, 105017 (2012).
[130] K.-I. Kondo, Confinement–deconfinement phase transition and gauge-invariant gluonic mass in Yang-Mills theory, arXiv:1508.02656.
[131] R. D. Pisarski and V. V. Skokov, Chiral matrix model of the semi-QGP in QCD, Phys. Rev. D **94**, 034015 (2016).
[132] H. Nishimura, R. D. Pisarski, and V. V. Skokov, Finite-temperature phase transitions of third and higher order in gauge theories at large N, Phys. Rev. D **97**, 036014 (2018).
[133] Y. Guo and Q. Du, Two-loop perturbative corrections to the constrained effective potential in thermal QCD, J. High Energy Phys. 05 (2019) 042.
[134] C. P. Korthals Altes, H. Nishimura, R. D. Pisarski, and V. V. Skokov, Free energy of a holonomous plasma, Phys. Rev. D **101**, 094025 (2020).
[135] Y. Hidaka and R. D. Pisarski, Effective models of a semi-quark-gluon plasma, Phys. Rev. D **104**, 074036 (2021).
[136] J. M. Maldacena, The large N limit of superconformal field theories and supergravity, Adv. Theor. Math. Phys. **2**, 231 (1998).
[137] S. S. Gubser, I. R. Klebanov, and A. M. Polyakov, Gauge theory correlators from noncritical string theory, Phys. Lett. B **428**, 105 (1998).
[138] E. Witten, Anti-de Sitter space and holography, Adv. Theor. Math. Phys. **2**, 253 (1998).
[139] O. Aharony, S. S. Gubser, J. M. Maldacena, H. Ooguri, and Y. Oz, Large N field theories, string theory and gravity, Phys. Rep. **323**, 183 (2000).
[140] E. Witten, Anti-de Sitter space, thermal phase transition, and confinement in gauge theories, Adv. Theor. Math. Phys. **2**, 505 (1998).
[141] I. R. Klebanov and M. J. Strassler, Supergravity and a confining gauge theory: Duality cascades and chi SB resolution of naked singularities, J. High Energy Phys. 08 (2000) 052.
[142] J. M. Maldacena and C. Nunez, Towards the large N limit of pure $N = 1$ superYang-Mills, Phys. Rev. Lett. **86**, 588 (2001).
[143] A. H. Chamseddine and M. S. Volkov, Non-Abelian BPS monopoles in $N = 4$ gauged supergravity, Phys. Rev. Lett. **79**, 3343 (1997).

[144] J. Babington, J. Erdmenger, N. J. Evans, Z. Guralnik, and I. Kirsch, Chiral symmetry breaking and pions in nonsupersymmetric gauge / gravity duals, Phys. Rev. D **69**, 066007 (2004).

[145] A. Butti, M. Grana, R. Minasian, M. Petrini, and A. Zaffaroni, The baryonic branch of Klebanov-Strassler solution: A supersymmetric family of $SU(3)$ structure backgrounds, J. High Energy Phys. 03 (2005) 069.

[146] R. C. Brower, S. D. Mathur, and C.-I. Tan, Glueball spectrum for QCD from AdS supergravity duality, Nucl. Phys. **B587**, 249 (2000).

[147] A. Karch and E. Katz, Adding flavor to AdS/CFT, J. High Energy Phys. 06 (2002) 043.

[148] M. Kruczenski, D. Mateos, R. C. Myers, and D. J. Winters, Meson spectroscopy in AdS/CFT with flavor, J. High Energy Phys. 07 (2003) 049.

[149] T. Sakai and S. Sugimoto, Low energy hadron physics in holographic QCD, Prog. Theor. Phys. **113**, 843 (2005).

[150] T. Sakai and S. Sugimoto, More on a holographic dual of QCD, Prog. Theor. Phys. **114**, 1083 (2005).

[151] F. Bigazzi, A. Caddeo, A. L. Cotrone, and A. Paredes, Fate of false vacua in holographic first-order phase transitions, J. High Energy Phys. 12 (2020) 200.

[152] F. R. Ares, M. Hindmarsh, C. Hoyos, and N. Jokela, Gravitational waves from a holographic phase transition, J. High Energy Phys. 21 (2020) 100.

[153] Y. Bea, J. Casalderrey-Solana, T. Giannakopoulos, D. Mateos, M. Sanchez-Garitaonandia, and M. Zilhão, Bubble wall velocity from holography, Phys. Rev. D **104**, L121903 (2021).

[154] F. Bigazzi, A. Caddeo, T. Canneti, and A. L. Cotrone, Bubble wall velocity at strong coupling, J. High Energy Phys. 08 (2021) 090.

[155] O. Henriksson, Black brane evaporation through D-brane bubble nucleation, Phys. Rev. D **105**, L041901 (2022).

[156] F. R. Ares, O. Henriksson, M. Hindmarsh, C. Hoyos, and N. Jokela, Effective actions and bubble nucleation from holography, Phys. Rev. D **105**, 066020 (2022).

[157] F. R. Ares, O. Henriksson, M. Hindmarsh, C. Hoyos, and N. Jokela, Gravitational waves at strong coupling from an effective action, Phys. Rev. Lett. **128**, 131101 (2022).

[158] E. Morgante, N. Ramberg, and P. Schwaller, Gravitational waves from dark $SU(3)$ Yang-Mills theory, Phys. Rev. D **107**, 036010 (2023).

[159] Y. Bea, J. Casalderrey-Solana, T. Giannakopoulos, A. Jansen, S. Krippendorf, D. Mateos, M.l Sanchez-Garitaonandia, and M. Zilhão, Spinodal gravitational waves, J. High Energy Phys. 11 (2025) 093.

[160] Y. Bea, J. Casalderrey-Solana, T. Giannakopoulos, A. Jansen, D. Mateos, M. Sanchez-Garitaonandia, and M. Zilhão, Holographic bubbles with Jecco: Expanding, collapsing and critical, J. High Energy Phys. 09 (2022) 008.

[161] Y. Bea, R. Jimenez, D. Mateos, S. Liu, P. Protopapas, P. Tarancón-Álvarez, and P. Tejerina-Pérez, Gravitational duals from equations of state, J. High Energy Phys. 07 (2024) 087.

[162] Y. Bea, J. Casalderrey-Solana, D. Mateos, and M. Sanchez-Garitaonandia, Hydrodynamics of relativistic superheated bubbles, Phys. Rev. D **112**, 114041 (2025).

[163] Y. Bea, M. Giliberti, D. Mateos, M. Sanchez-Garitaonandia, A. Serantes, and M. Zilhão, Bubble dynamics in a QCD-like phase diagram, J. High Energy Phys. 04 (2026) 013.

[164] F. Wang and D. P. Landau, Efficient, multiple-range random walk algorithm to calculate the density of states, Phys. Rev. Lett. **86**, 2050 (2001).

[165] K. Langfeld, B. Lucini, and A. Rago, The density of states in gauge theories, Phys. Rev. Lett. **109**, 111601 (2012).

[166] K. Langfeld and J. M. Pawlowski, Two-color QCD with heavy quarks at finite densities, Phys. Rev. D **88**, 071502 (2013).

[167] K. Langfeld, B. Lucini, R. Pellegrini, and A. Rago, An efficient algorithm for numerical computations of continuous densities of states, Eur. Phys. J. C **76**, 306 (2016).

[168] G. Cossu, D. Lancastera, B. Lucini, R. Pellegrini, and A. Rago, Ergodic sampling of the topological charge using the density of states, Eur. Phys. J. C **81**, 375 (2021).

[169] M. D'Elia, K. Langfeld, and B. Lucini, *Stochastic Methods in Scientific Computing*, Numerical Analysis and Scientific Computing Series (CRC Press LLC, Boca Raton, 2024).

[170] D. Mason, B. Lucini, M. Piai, E. Rinaldi, and D. Vadacchino, The density of states method in Yang-Mills theories and first order phase transitions, EPJ Web Conf. **274**, 08007 (2022).

[171] D. Mason, B. Lucini, M. Piai, E. Rinaldi, and D. Vadacchino, The density of state method for first-order phase transitions in Yang-Mills theories, Proc. Sci. LATTICE2022 (**2023**) 216 [arXiv:2212.01074].

[172] B. Lucini, D. Mason, M. Piai, E. Rinaldi, and D. Vadacchino, First-order phase transitions in Yang-Mills theories and the density of state method, Phys. Rev. D **108**, 074517 (2023).

[173] E. Bennett, B. Lucini, D. Mason, M. Piai, E. Rinaldi, and D. Vadacchino, Density of states method for symplectic gauge theories at finite temperature, Phys. Rev. D **111**, 114511 (2025).

[174] F. Springer and D. Schaich, Density of states for gravitational waves, Proc. Sci. LATTICE2021 (**2022**) 043 [arXiv:2112.11868].

[175] F. Springer and D. Schaich, Progress applying density of states for gravitational waves, EPJ Web Conf. **274**, 08008 (2022).

[176] Lattice Strong Dynamics (LSD) Collaboration, Advances in using density of states for large-N Yang–Mills, Proc. Sci. LATTICE2022 (**2023**) 223 [arXiv:2303.01149].

[177] Lattice Strong Dynamics (LSD) Collaboration, First-order bulk transitions in large-N lattice Yang–Mills theories using the density of states, arXiv:2311.10243.

[178] E. Bennett, D. K. Hong, J.-W. Lee, C. J. D. Lin, B. Lucini, M. Piai, and D. Vadacchino, Sp(4) gauge theory on the lattice: Towards SU(4)/Sp(4) composite Higgs (and beyond), J. High Energy Phys. 03 (2018) 185.

[179] E. Bennett, J. Holligan, D. K. Hong, J.-W. Lee, C. J. D. Lin, B. Lucini *et al.*, Color dependence of tensor and scalar glueball masses in Yang-Mills theories, Phys. Rev. D **102**, 011501 (2020).

[180] E. Bennett, J. Holligan, D. K. Hong, J.-W. Lee, C. J. D. Lin, B. Lucini *et al.*, Glueballs and strings in $Sp(2N)$ Yang-Mills theories, Phys. Rev. D **103**, 054509 (2021).

[181] E. Bennett, D. K. Hong, J.-W. Lee, C. J. D. Lin, B. Lucini, M. Piai, and D. Vadacchino, Color dependence of the topological susceptibility in Yang-Mills theories, Phys. Lett. B **835**, 137504 (2022).
[182] E. Bennett, D. K. Hong, J.-W. Lee, C. J. D. Lin, B. Lucini, M. Piai *et al.*, $Sp(2N)$ Yang-Mills theories on the lattice: Scale setting and topology, Phys. Rev. D **106**, 094503 (2022).
[183] J.-W. Lee, E. Bennett, D. K. Hong, C. J. D. Lin, B. Lucini, M. Piai *et al.*, Progress in the lattice simulations of $Sp(2N)$ gauge theories, Proc. Sci. LATTICE2018 (**2018**) 192 [arXiv:1811.00276].
[184] E. Bennett, D. K. Hong, J.-W. Lee, C. J. D. Lin, B. Lucini, M. Piai, and D. Vadacchino, Sp(4) gauge theories on the lattice: $N_f = 2$ dynamical fundamental fermions, J. High Energy Phys. 12 (2019) 053.
[185] E. Bennett, D. K. Hong, J.-W. Lee, C.-J. D. Lin, B. Lucini, M. Mesiti, M. Piai, J. Rantaharju, and D. Vadacchino, $Sp(4)$ gauge theories on the lattice: quenched fundamental and antisymmetric fermions, Phys. Rev. D **101**, 074516 (2020).
[186] E. Bennett, D. K. Hong, H. Hsiao, J.-W. Lee, C. J. D. Lin, B. Lucini *et al.*, Lattice studies of the $Sp(4)$ gauge theory with two fundamental and three antisymmetric Dirac fermions, Phys. Rev. D **106**, 014501 (2022).
[187] E. Bennett *et al.*, Symplectic lattice gauge theories in the grid framework: Approaching the conformal window, Phys. Rev. D **108**, 094508 (2023).
[188] E. Bennett, D. K. Hong, H. Hsiao, J.-W. Lee, C. J. D. Lin, B. Lucini *et al.*, Lattice investigations of the chimera baryon spectrum in the $Sp(4)$ gauge theory, Phys. Rev. D **109**, 094512 (2024).
[189] E. Bennett, J. Holligan, D. K. Hong, J.-W. Lee, C. J. D. Lin, B. Lucini *et al.*, Spectrum of mesons in quenched $Sp(2N)$ gauge theories, Phys. Rev. D **109**, 094517 (2024).
[190] E. Bennett *et al.*, Meson spectroscopy from spectral densities in lattice gauge theories, Phys. Rev. D **110**, 074509 (2024).
[191] E. Bennett, N. Forzano, D. K. Hong, H. Hsiao, J.-W. Lee, C. J. D. Lin, B. Lucini, M. Piai, D. Vadacchino, and F. Zierler, Mixing between flavor singlets in lattice gauge theories coupled to matter fields in multiple representations, Phys. Rev. D **110**, 074504 (2024).
[192] E. Bennett, D. K. Hong, H. Hsiao, J.-W. Lee, C. J. D. Lin, B. Lucini, M. Piai, and D. Vadacchino, Meson spectroscopy in the $Sp(4)$ gauge theory with three antisymmetric fermions, Phys. Rev. D **111**, 074511 (2025).
[193] E. Bennett *et al.*, Chimera baryons and mesons on the lattice: A spectral density analysis, Phys. Rev. D **112**, 074515 (2025).
[194] E. Bennett, J. Holligan, D. K. Hong, H. Hsiao, J.-W. Lee, C. J. D. Lin, B. Lucini, M. Mesiti, M. Piai, and D. Vadacchino, $Sp(2N)$ lattice gauge theories and extensions of the standard model of particle physics, Universe **9**, 236 (2023).
[195] D. K. Hong, J.-W. Lee, B. Lucini, M. Piai, and D. Vadacchino, Casimir scaling and Yang–Mills glueballs, Phys. Lett. B **775**, 89 (2017).
[196] E. Bennett, H. Hsiao, J.-W. Lee, B. Lucini, A. Maas, M. Piai, and F. Zierler, Singlets in gauge theories with fundamental matter, Phys. Rev. D **109**, 034504 (2024).
[197] Y. Dengler, A. Maas, and F. Zierler, Scattering of dark pions in $Sp(4)$ gauge theory, Phys. Rev. D **110**, 054513 (2024).
[198] L. Del Debbio, A. Patella, and C. Pica, Higher representations on the lattice: Numerical simulations. SU(2) with adjoint fermions, Phys. Rev. D **81**, 094503 (2010).
[199] GitHub—claudiopica/HiRep: HiRep repository—github.com., https://github.com/claudiopica/HiRep.
[200] GitHub—sa2c/HiRep: HiRep repository—github.com., https://github.com/sa2c/HiRep.
[201] D. Mason, B. Lucini, M. Piai, D. Vadacchino, and E. Rinaldi, First-order phase transitions in Yang-Mills theories and the density of state method—HiRep LLR code v1.0.0, 2023. 10.5281/zenodo.8134756.
[202] D. Mason, E. Bennett, B. Lucini, M. Piai, D. Vadacchino, and E. Rinaldi, The density of states method for symplectic gauge theories at finite temperature—HiRep LLR code v1.1.0, 2024. 10.5281/zenodo.13807993.
[203] H. Robbins and S. Monro, A stochastic approximation method, Ann. Math. Stat. **22**, 400 (1951).
[204] R. H. Swendsen and J.-S. Wang, Replica Monte Carlo simulation of spin-glasses, Phys. Rev. Lett. **57**, 2607 (1986).
[205] T. Vogel, Y. Wai Li, and D. P Landau, A practical guide to replica-exchange wang—landau simulations, J. Phys. Conf. Ser. **1012**, 012003 (2018).
[206] E. Bennett, The TELOS Collaboration approach to reproducibility and open science, arXiv:2504.01876.
[207] P. de Forcrand, B. Lucini, and M. Vettorazzo, Measuring interface tensions in 4D $SU(N)$ lattice gauge theories, Nucl. Phys. B, Proc. Suppl. **140**, 647 (2005).
[208] T. Rindlisbacher, K. Rummukainen, and A. Salami, Confined-deconfined interface tension and latent heat in $SU(N)$ gauge theory, Phys. Rev. D **112**, 114507 (2025).
[209] Y. Iwasaki, K. Kanaya, L. Karkkainen, K. Rummukainen, and T. Yoshie, Interface tension in quenched QCD, Phys. Rev. D **49**, 3540 (1994).
[210] B. Grossmann, M. L. Laursen, T. Trappenberg, and U. J. Wiese, The interface tension in quenched QCD at the deconfinement temperature, Nucl. Phys. B, Proc. Suppl. **30**, 869 (1993).
[211] B. Beinlich, F. Karsch, and A. Peikert, $SU(3)$ latent heat and surface tension from tree level and tadpole improved actions, Phys. Lett. B **390**, 268 (1997).
[212] E. Bennett, B. Lucini, D. Mason, M. Piai, E. Rinaldi, D. Vadacchino *et al.*, Analysis release—finite-temperature Yang-Mills theories with the density of states method: Towards the continuum limit (2025), 10.5281/zenodo.16579683.
[213] www.dirac.ac.uk.
[214] E. Bennett, B. Lucini, D. Mason, M. Piai, E. Rinaldi, D. Vadacchino *et al.*, Data release—finite-temperature Yang-Mills theories with the density of states method: Towards the continuum limit (2025), 10.5281/zenodo.19449913.
[215] W. Janke, First-order phase transitions, in *Computer Simulations of Surfaces and Interfaces*, edited by B. Dünweg, D. P. Landau, and A. I. Milchev (Springer Netherlands, Dordrecht, 2003), pp. 111–135.